Alfvén Acoustic Channel for Ion Energy in High-Beta Tokamak Plasmas

Andreas Bierwage,[1,*] Nobuyuki Aiba,[1] and Kouji Shinohara[2]
[1]Japan Atomic Energy Agency, Rokkasho, Aomori 039-3212, Japan
[2]Japan Atomic Energy Agency, Naka, Ibaraki 311-0193, Japan
(Received 9 September 2014; published 9 January 2015)

When the plasma beta (ratio of thermal to magnetic pressure) in the core of a tokamak is raised to values of several percent, as required for a thermonuclear fusion reactor, continuous spectra of long-wavelength slow magnetosonic waves enter the frequency band occupied by continuous spectra of shear Alfvén waves. It is found that these two branches can couple strongly, so that Alfvén modes that are resonantly driven by suprathermal ions transfer some of their energy to sound waves. Since sound waves are heavily damped by thermal ion Landau resonances, these results reveal a new energy channel that contributes to the damping of Alfvénic instabilities and the noncollisional heating of bulk ions, with potentially important consequences for confinement and fusion performance.

DOI: 10.1103/PhysRevLett.114.015002 PACS numbers: 52.55.Fa, 52.35.Bj, 52.55.Pi, 52.65.Ww

The realization of self-sustained "burning" fusion conditions in tokamaks relies on, among other factors, the achievement of high plasma beta (β) values around 5%, and on the efficient heating of the bulk plasma by fusion products, namely, fast alpha particles. Besides direct collisional energy transfer, the fast ions may transfer their energy to kinetically damped waves. This noncollisional heating via wave-particle interactions is known as "alpha channeling" [1,2]. Fast ions resonate with shear Alfvén waves (SAW), so noncollisional heating occurs, for instance, when the energy deposited by the fast ions in the SAW continua is absorbed by the bulk plasma through continuum damping (kinetic damping after phase mixing). However, the resonant drive may overcome continuum damping and destabilize energetic particle modes (EPM) [3], causing premature loss of fast ions from the plasma core before their energy is absorbed [4]. This has raised skepticism about the importance of alpha channeling, but there are at least two reasons for maintaining interest in this subject: (i) reliable quantitative predictions remain to be made, especially for burning plasmas, and (ii) there are yet unknown energy channels.

Concerning point (i), both the amount of fast-ion profile flattening and the amount of energy channeled to bulk ions depend on the structure, frequency, and amplitude of the modes, evolving nonlinearly in the presence of resonances and competing sources and sinks. Therefore, reliable predictions for alpha channeling will require self-consistent long-time simulations, which is an active area of research [5,6]. Concerning point (ii), in order to extract useful information from such comprehensive simulations, it is important to go beyond the common study of instabilities and develop a broader understanding of the energy flows in the system, including those through the rich spectrum of damped modes. The discovery of such an energy channel is reported here.

In this Letter, it is demonstrated numerically that, in high-beta tokamak plasmas, fast ions may transfer energy to bulk ions through the resonant excitation of modes that reside inside the SAW continuum and are coupled to slow magnetosonic waves (SMW). At low β (<1%), such coupling occurs only inside the low-frequency gap of the SAW continuum opened by finite plasma compressibility [7], where it gives rise to Alfvén-acoustic gap modes [8–10]. These low-frequency modes are strongly affected by kinetic effects [11–13]. We show that, when β is raised to higher values (>1%), maxima of SMW continua rise above the gap and enter the SAW continua. These maxima support radially extended standing waves, named global slow magnetosonic eigenmodes (GSME), which are capable of coupling to nearby SAW continua and tapping energy from EPMs. Ion Landau damping of SMWs [14] will transfer that energy to bulk ions.

As a working example, we use JT-60U shot E039672, which was part of an experimental campaign performed to explore fast-ion dynamics in parameter regimes relevant to burning plasmas by producing high values of beta and injecting a pair of 400 keV negative-ion-based neutral beams (NNB) [15]. Figure 1 shows the numerically reconstructed equilibrium configuration, with $\beta_0 = 3.6\%$ at the center ($r = 0$). After applying an initial perturbation, the plasma response is simulated by solving the full set of single-fluid magnetohydrodynamic (MHD) equations as an initial value problem, using the MHD module of the code MEGA [16,17] and a setup similar to that in Refs. [18,19]. The fluctuations of the MHD velocity vector $\delta \boldsymbol{U}$ and pressure δP are measured, mapped to magnetic flux coordinates (r, ϑ, ζ), and Fourier-analyzed in space as

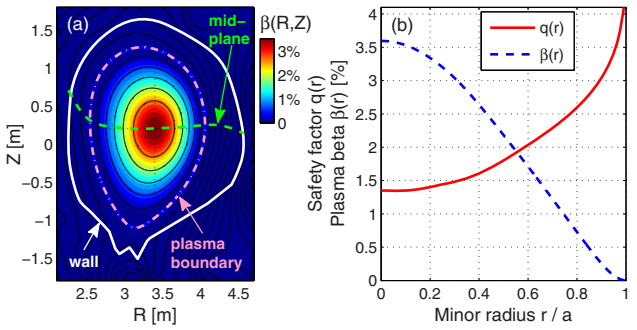

FIG. 1 (color online). MHD equilibrium. (a) Pressure contours. (b) Radial profiles of the safety factor $q(r)$ and plasma beta $\beta(r)$.

$$\delta \boldsymbol{U}(r,\vartheta,\zeta,t) = \sum_{n=-n_{\max}}^{n_{\max}} e^{-in\zeta} \underbrace{\sum_{m=0}^{m_{\max}} \delta \boldsymbol{u}_{m,n}(r,t) e^{im\vartheta}}_{\delta \boldsymbol{u}_n(r,\vartheta,t)}, \qquad (1)$$

where $0 \le r \le a$ is the minor radius, and m and n are the mode numbers for the poloidal and toroidal angles ϑ and ζ. In the following, the time t and angular frequency ω are normalized by the Alfvén frequency at the plasma center, $\omega_{A0} = v_{A0}/R_0$, and the minor radial coordinate r is normalized by its boundary value a. The aspect ratio of the major and minor radii of the plasma is $R_0/a \approx 3.4$. We focus on long-wavelength modes in the plasma core ($nq \sim m \lesssim 6$) with frequencies in the SAW continuum, which justifies the use of MHD as a discovery tool [20].

Figure 2 shows spectrograms of MHD velocity fluctuations with toroidal mode number $n = 3$, which are computed on the outer midplane ($\vartheta = 0$) as

$$\delta \boldsymbol{u}_n(r,\omega) = \int dt \delta \boldsymbol{u}_n(r,0,t) H(t-t_0) e^{i\omega t}, \qquad (2)$$

where $H(t-t_0)$ is a Hanning window for the Fourier transform of the time interval $t_0 - t_{\rm win}/2 \le t \le t_0 + t_{\rm win}/2$. The spectrum of the toroidal component δu_ζ in Fig. 2(a) is dominated by SMWs and the radial component δu_r in Fig. 2(b) by SAWs. The signals are interpreted by comparison with continuous spectra computed as described in Refs. [7,21]. The full MHD continua in Fig. 2(a) contain both branches with Alfvénic (A) and sound (S) polarizations, the frequencies of which will be denoted by $\omega_A(r)$ and $\omega_S(r)$. A slow-sound approximation allows us to isolate the Alfvén continua $\omega_A(r)$ shown in Fig. 2(b). Some branches are labeled with poloidal mode numbers $m^{\pm}_{S/A}$, where the superscripts identify the sign of $k_\parallel$, the wave number parallel to the magnetic field $\boldsymbol{B}$, which is defined as

$$-i\frac{\boldsymbol{B}}{B}\cdot\nabla \leftrightarrow k_\parallel(r) = \frac{1}{R_0}\left(n - \frac{m^{\pm}}{q(r)}\right) \gtrless 0. \qquad (3)$$

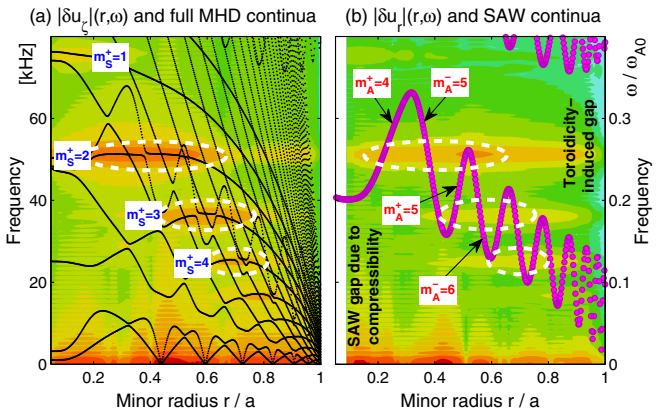

FIG. 2 (color online). Spectrograms of MHD responses for $\beta_0 = 3.6\%$ and $n = 3$, computed using Eq. (2) with $t_{\rm win} = 1100$ for (a) the toroidal δu_ζ and (b) radial velocity component δu_r. The color scale is logarithmic, with strongly responsive regions (or slowly decaying modes) appearing red to orange. Lines and dots indicate full MHD continua in (a) and SAW continua in (b).

Figure 1(b) shows that the $q(r)$ profile, which measures the magnetic field pitch, rises with increasing radius r, whereas $\beta(r)$ decreases. This produces maxima on sound continuum branches $\omega_S(r)$ with $k_\parallel > 0$. Particular attention should be paid to the maxima of the $\omega_S(r)$ branches with $m^+_S = 2, 3$, and 4 in Fig. 2(a): they overlap with Alfvén continua $\omega_A(r)$ and exhibit strong responses both in the δu_ζ and δu_r spectra in Figs. 2(a) and 2(b). These couplings and the associated modes, which are encircled with dashed lines in Fig. 2, are the subject of this Letter.

In order to study the role of β, a second equilibrium with profiles similar to Fig. 1 but lower pressure was constructed. The MHD responses obtained for $\beta_0 = 1.7\%$ and 3.6% are compared in Fig. 3. The δu_r spectra in Figs. 3(a) and 3(b) show how three discrete MHD modes labeled M1, M2, and M3 are locked to the maxima of the sound continua $\omega_S(r)$ with poloidal mode numbers $m^+_S = 1, 2$, and 3, which means that the mode frequencies ω scale approximately as $(\beta\Gamma)^{1/2}$. This estimate is based on the SMW dispersion relation in the local limit, $\omega_S^2 = k_{\parallel S}^2 v_A^2 \beta\Gamma/2$. Here, the specific heat ratio is $\Gamma = 5/3$. Ignoring geometric effects (toroidicity, shaping), the condition $\omega_S^2 \sim \omega_A^2 = k_{\parallel A}^2 v_A^2$ can be written as

$$|nq(r) - m_A|^2 / |nq(r) - m_S|^2 \sim \beta(r)\Gamma/2, \qquad (4)$$

and determines how large β must be to allow the frequencies of harmonics (m_S, n) and (m_A, n) to match. Mode M2 in Fig. 3 satisfies Eq. (4) up to a factor 2. The circumstances under which this necessary condition becomes sufficient for SMWs and SAWs to couple strongly and form a discrete MHD mode remain to be understood. Apparently, $d\omega_S/dr \approx 0$ is an important criterion. Geometric and kinetic effects may also play a role.

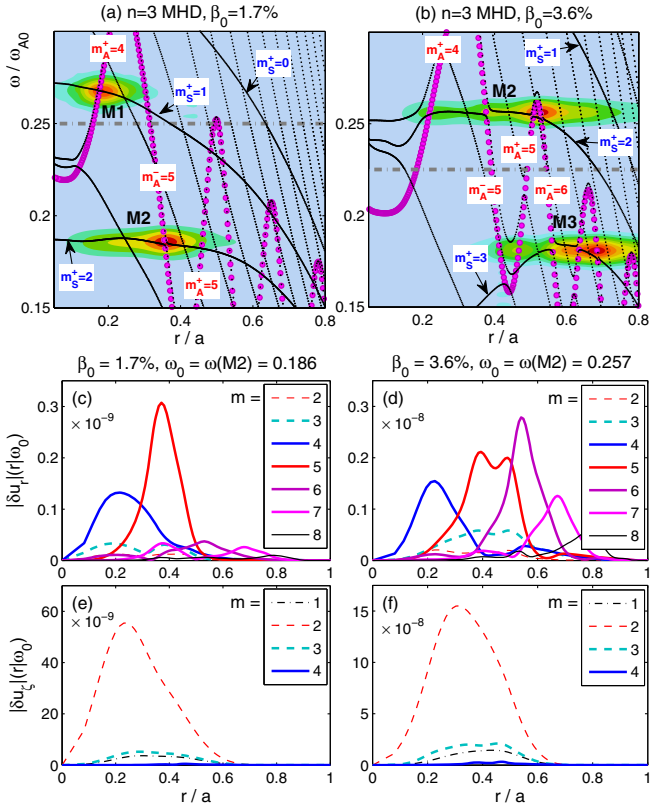

FIG. 3 (color online). Comparison of $n = 3$ MHD responses for $\beta_0 = 1.7\%$ and 3.6%. (a),(b) Contours of spectrograms $|\delta u_r|(r, \omega)$ with $t_{\rm win} = 1100$. The contours above and below the dash-dotted lines have independent linear color scales. Lines and dots indicate continuous spectra as in Fig. 2. (c)–(f) Radial structures of poloidal harmonics of $|\delta u_r|(r|\omega_0)$ and $|\delta u_\zeta|(r|\omega_0)$ for mode M2 of (a) and (b). These are obtained by analyzing slices of data at $\omega_0 = 0.186$ (c),(e) and $\omega_0 = 0.257$ (d),(f).

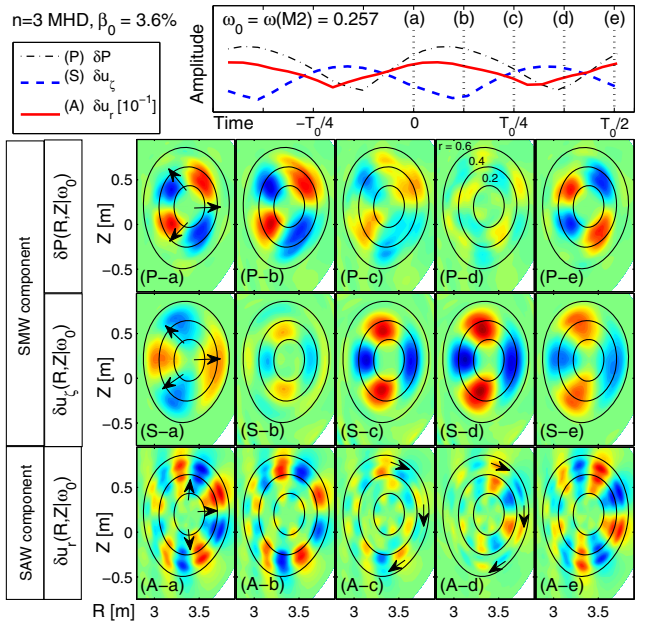

FIG. 4 (color online). Global structure and evolution of mode M2 found in the $n = 3$ MHD response for $\beta_0 = 3.6\%$. The top panel shows the evolution of the peak amplitudes during one wave period $T_0 = 2\pi/\omega_0 = 22.4$ for the pressure δP (P), and the velocity components δu_ζ (S: sound), and δu_r (A: Alfvénic) that oscillate with frequency $\omega_0 = \omega(\mathrm{M2}) = 0.257$. Labeled (a)–(e), five snapshots of $\delta P(R, Z|\omega_0)$, $\delta u_\zeta(R, Z|\omega_0)$, and $\delta u_r(R, Z|\omega_0)$ are shown as color contour plots. The black ellipses indicate magnetic flux surfaces at $r = 0.2$, 0.4, and 0.6. Arrows indicate the (real or apparent) propagation of the structures.

The radial profiles of individual poloidal harmonics, from which mode M2 is composed, are shown in Fig. 3(c)–(f). One can see how the dominant poloidal mode numbers are determined by the nearby continua. For $\beta_0 = 1.7\%$, the frequency analyzed is $\omega_0 = \omega(\mathrm{M2}) = 0.186$, and Fig. 3(c) shows that the structure of $\delta u_r(r|\omega_0)$ is dominated by the $m = 5$ harmonic. For $\beta_0 = 3.6\%$, the frequency is $\omega_0 = \omega(\mathrm{M2}) = 0.257$, and Fig. 3(d) shows that $\delta u_r(r|\omega_0)$ is dominated by $m = 5$ and 6. The magnitude of the $m = 2$ harmonic in Figs. 3(c) and 3(d) is smaller than that of $m = 5$ by a factor ~0.05–0.1, so the radial velocity component δu_r of mode M2 is dominated by the SAW. In contrast, the toroidal velocity component δu_ζ in Figs. 3(e) and 3(f) is clearly dominated by the SMW with $m = 2$.

The global structure of mode M2 and its evolution for $\beta_0 = 3.6\%$ is shown in Fig. 4. During one half of the wave period $T_0 = 2\pi/\omega_0 = 22.4$, where $\omega_0 = \omega(\mathrm{M2}) = 0.257$, five snapshots are taken and labeled (a)–(e) as indicated in the top panel of Fig. 4. Rows (P) and (S) of Fig. 4 show that the SMW component of the mode has the form of a standing sound wave with dominant harmonic $(m, n) = (2, 3)$. Naturally, the pressure fluctuation δP lags behind the toroidal velocity fluctuation δu_ζ by $T_0/4$. As indicated by arrows in snapshots (P-a) and (S-a), there is an apparent outward propagation of the wave front, which indicates that the standing SMWs at larger radii lag behind those at smaller radii. The radial velocity fluctuation δu_r, which is plotted in row (A) of Fig. 4 and represents the SAW component of the mode, exhibits similar pulses in the region $0.2 \lesssim r \lesssim 0.6$. This suggests that the pressure fluctuation of the SMW component drives the SAW component. Between successive pulses, one can observe a clockwise rotation of the δu_r fluctuations in the region $0.4 \lesssim r \lesssim 0.6$, as indicated by the arrows in Fig. 4, (A-c) and (A-d). This is the typical behavior of a SAW when it propagates parallel to $\boldsymbol{B}$. The above results may be summarized as follows.

1. Discrete MHD modes with slow-sound polarization are found in regions where the frequencies $\omega_S(r)$ of SMWs with poloidal mode number m_S^+ have a weak radial dependence, $d\omega_S/dr \approx 0$ [Fig. 2(a)]. Our acronym for such a standing SMW [Fig. 4] is global slow magnetosonic eigenmode (GSME).

2. For $\beta \gtrsim 1\%$, GSMEs overlap with and couple to SAW continua $\omega_A(r)$ [Fig. 2(b)]. This coupling manifests itself in

the excitation of SAWs [Fig. 3], which exhibit pulsations as well as propagation parallel to $\boldsymbol{B}$ [Fig. 4]. The frequency of the resulting discrete mode is controlled by the β-dependent frequency of its GSME component, so it is called beta-induced Alfvén continuum mode (BACM).

3. The Alfvénic δu_r component of a BACM reflects the structure of the SAW spectrum and its geometric couplings. For instance, near an accumulation point of the toroidicity-induced gap [cf. Fig. 2(b)], δu_r contains multiple poloidal harmonics m_A with comparable amplitudes [Fig. 3(d)], so that it bears similarity to a toroidicity-induced Alfvén eigenmode (TAE) [22] and its "kinetic" counterparts (KTAE) [23], here produced by resistivity [22].

The energy transfer between SMW and SAW, which underlies the formation of BACMs, works also in the opposite direction: SMWs are excited when the SAW component of a BACM is driven by fast ions. This is demonstrated in Fig. 5, where the spectrograms and mode structures of fast-ion-driven instabilities during their exponential growth phase are shown. The simulations were performed with the hybrid code MEGA [16,17], using the NNB ion distribution shown in Fig. 4(d) of Ref. [19] and the same cases as in Fig. 3 above.

For $\beta_0 = 1.7\%$, Figs. 5(a) and 5(c) show that the NB-driven mode has a peak near $(r, \omega) \approx (0.3, 0.29)$, which is close to mode M1 associated with the $m_S^+ = 1$ branch in Fig. 3(a). Indeed, a strong $m = 1$ harmonic is present in the δu_ζ component in Fig. 5(e). For $\beta_0 = 3.6\%$, Figs. 5(b) and 5(d) show that the NB-driven mode has a peak near $(r, \omega) \approx (0.4, 0.28)$, which is close to mode M2 associated with the $m_S^+ = 2$ branch in Fig. 3(b). Indeed, a strong $m = 2$ harmonic is present in the δu_ζ component Fig. 5(f). These results show that EPMs couple to nearby BACMs, which means that energy flows from the EPM (resonantly driven SAW) to parasitic SMWs.

In summary, it was demonstrated numerically that, in a tokamak with sufficiently high β (here 1.7–3.6%), maxima of sound continua $\omega_S(r)$ and the associated global slow magnetosonic eigenmodes can overlap with Alfvén continua $\omega_A(r)$. The two branches are found to couple, producing GSMEs with Alfvénic components, which we call beta-induced Alfvén continuum modes. Finally, it was demonstrated that fast-ion-driven shear Alfvén instabilities can couple to sound waves via BACMs. The influence of kinetic effects on the efficiency of such couplings remains to be quantified. Apart from this, the use of MHD is justified by the fact that the modes studied are localized in the plasma core, have long wavelengths, and frequencies above the SAW gap opened by compressibility [20].

The above results have potentially important implications. Within the resistive MHD model used here, the exponential decay rate of the BACM pulses in Fig. 4 is $\gamma \sim -10^{-3}$. The exaggerated resonant fast-ion drive in the initial-value simulations reported in Fig. 5 easily exceeds that by an order of magnitude. In self-consistent long-time simulations [5,6], the drive does not usually grow that strong. Moreover, when kinetic thermal ion effects are included, SMWs will be subject to ion Landau damping, which is strong unless $T_e \gg T_i$ [14]. Therefore, it is expected that, in present-day beam-heated tokamaks ($T_e \lesssim T_i$) and burning plasmas ($T_e \gtrsim T_i$), fast-ion-driven modes that overlap with BACMs in radius r and frequency ω are subject to enhanced damping. Consequently, BACMs may reduce the amount of energy contained in undesirable Alfvénic fluctuations while enhancing desirable noncollisional heating of bulk ions. In other words, BACMs act as channels that convert expansion free energy contained in the gradient of the fast-ion pressure profile into thermal energy of bulk ions. These effects and their implications for the realization of burning plasmas should be examined through further research.

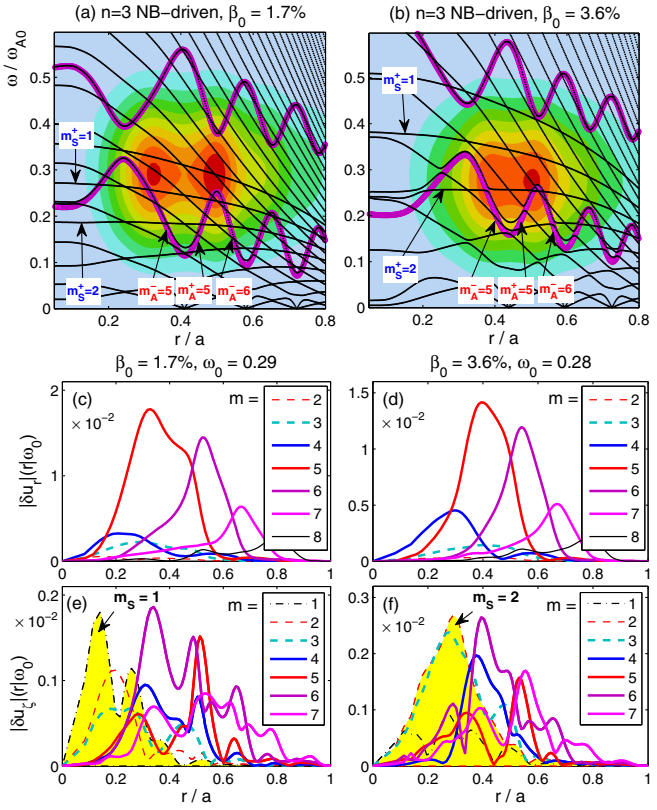

FIG. 5 (color online). Comparison of NB-driven $n = 3$ modes for $\beta_0 = 1.7\%$ and 3.6%. Arranged like Fig. 3. (a),(b) Contour plots of spectrograms $|\delta u_r|(r, \omega)$ computed with $t_{\text{win}} = 50$. (c)–(f) Radial structures of poloidal harmonics of $|\delta u_r|(r|\omega_0)$ and $|\delta u_\zeta|(r|\omega_0)$ for frequencies ω_0 inferred from (a) and (b). Harmonics of δu_ζ belonging to BACMs are shaded in (e),(f).

One of the authors (A. B.) thanks Yasushi Todo (NIFS, Japan) for providing the code MEGA and useful discussions. Further useful discussions with Masatoshi Yagi (JAEA, Japan) are thankfully acknowledged. This work was partly supported by Grant-in-Aid for Scientific Research from the Japan Society for the Promotion of

Science (JSPS), Grant No. 25820443. The simulations were carried out using the supercomputer systems Fujitsu BX-900 at JAEA, Ibaraki, Japan, and HELIOS at IFERC, Aomori, Japan, under the Broader Approach collaboration between Euratom and Japan, implemented by Fusion for Energy and JAEA.

*Corresponding author.
bierwage.andreas@jaea.go.jp

[1] N. J. Fisch and J. M. Rax, Phys. Rev. Lett. **69**, 612 (1992).
[2] N. J. Fisch, Trans. Fusion Sci. Tech. **51**, 1 (2007).
[3] L. Chen, Phys. Plasmas **1**, 1519 (1994).
[4] M. Ishikawa *et al.*, Nucl. Fusion **45**, 1474 (2005).
[5] Y. Todo, M. A. Van Zeeland, A. Bierwage, and W. W. Heidbrink, Nucl. Fusion **54**, 104012 (2014).
[6] A. Bierwage, K. Shinohara, Y. Todo, and M. Yagi, in *Proceedings of the 25th IAEA Fusion Energy Conference, St. Petersburg, Russia, 2014* (International Atomic Energy Agency, Vienna, 2015).
[7] C. Z. Cheng and M. S. Chance, Phys. Fluids **29**, 3695 (1986).
[8] N. N. Gorelenkov, H. L. Berk, E. Fredrickson, S. E. Sharapov, and JET EFDA Contributors, Phys. Lett. A **370**, 70 (2007).
[9] N. N. Gorelenkov, H. L. Berk, N. A. Crocker, E. D. Fredrickson, S. Kaye, S. Kubota, H. Park, W. Peebles, S. A. Sabbagh, S. E. Sharapov, D. Stutmat, K. Tritz, F. M. Levinton, H. Yuh, the NSTX Team, and JET EFDA Contributors, Plasma Phys. Controlled Fusion **49**, B371 (2007).
[10] N. N. Gorelenkov, M. A. Van Zeeland, H. L. Berk, N. A. Crocker, D. Darrow, E. Fredrickson, G.-Y. Fu, W. W. Heidbrink, J. Menard, and R. Nazikian, Phys. Plasmas **16**, 056107 (2009).
[11] F. Zonca, L. Chen, and R. A. Santoro, Plasma Phys. Controlled Fusion **38**, 2011 (1996).
[12] D. Curran, Ph. Lauber, P. J. Mc Carthy, S. da Graca, V. Igochine, and the ASDEX Upgrade Team, Plasma Phys. Controlled Fusion **54**, 055001 (2012).
[13] I. Chavdarovski and F. Zonca, Phys. Plasmas **21**, 052506 (2014).
[14] *Collective Oscillations in Plasma*, edited by A. I. Akhiezer, I. A. Akhiezer, R. V. Polovin, A. G. Sitenko, and K. N. Stepanov (Pergamon, New York, 1967), p. 62, 86.
[15] K. Shinohara, M. Takechi, M. Ishikawa, Y. Kusama, A. Morioka, N. Oyama, K. Tobita, T. Ozeki, N. N. Gorelenkov, C. Z. Cheng, G. J. Kramer, and R. Nazikian, and the JT-60 Team, Nucl. Fusion **42**, 942 (2002).
[16] Y. Todo and T. Sato, Phys. Plasmas **5**, 1321 (1998).
[17] Y. Todo, K. Shinohara, M. Takechi, and M. Ishikawa, Phys. Plasmas **12**, 012503 (2005).
[18] A. Bierwage, K. Shinohara, N. Aiba, and Y. Todo, Nucl. Fusion **53**, 073007 (2013).
[19] A. Bierwage, Y. Todo, N. Aiba, and K. Shinohara, Nucl. Fusion **54**, 104001 (2014).
[20] Compared to the thermal ion Larmor radius ρ_{Li}, the wave numbers $k_\perp \sim nq/r$ satisfy $k_\perp \rho_{\mathrm{Li}} < 0.1$. Small-scale structures produced by phase mixing and nonlinearities are dissipated through resistivity and viscosity. The frequencies lie inside the SAW continuum, above the gap associated with plasma compressibility, so the diamagnetic frequency shift (here, $\omega_{*i}/\omega \lesssim 0.18$) and the modification of the effective plasma inertia due to magnetic trapping of ions [13] are regarded as negligible quantitative corrections. Resonances and phase-mixing in velocity space do not alter the structure of the continuous spectra.
[21] W. Deng, Z. Lin, I. Holod, Z. Wang, Y. Xiao, and H. Zhang, Nucl. Fusion **52**, 043006 (2012).
[22] C. Z. Cheng, L. Chen, and M. S. Chance, Ann. Phys. (Berlin) **161**, 21 (1985).
[23] R. R. Mett and S. M. Mahajan, Phys. Fluids B **4**, 2885 (1992).